A phenomenological cohesive model of ferroelectric fatigue

I. Arias [b] S. Serebrinsky [a],* M. Ortiz [a]

[a]*Division of Engineering and Applied Science, California Institute of Technology, Pasadena, CA 91125, USA*

[b]*Dep. de Matemàtica Aplicada III, Universitat Politècnica de Catalunya, Barcelona 08034, Spain*

Abstract

We develop a phenomenological model of electro-mechanical ferroelectric fatigue based on a ferroelectric cohesive law that couples mechanical displacement and electric-potential discontinuity to mechanical tractions and surface-charge density. The ferroelectric cohesive law exhibits a monotonic envelope and loading-unloading hysteresis. The model is applicable whenever the changes in properties leading to fatigue are localized in one or more planar-like regions, modelled by the cohesive surfaces. We validate the model against experimental data for a simple test configuration consisting of an infinite slab acted upon by an oscillatory voltage differential across the slab and otherwise stress free. The model captures salient features of the experimental record including: the existence of a threshold nominal field for the onset of fatigue; the dependence of the threshold on the applied-field frequency; the dependence of fatigue life on the amplitude of the nominal field; and the dependence of the coercive field on the size of the component, or *size effect*. Our results, although not conclusive, indicate that planar-like regions affected by cycling may lead to the observed fatigue in tetragonal PZT.

Key words: ferroelectricity, fatigue, fracture, nucleation, cohesive

1 Introduction

Ferroelectric materials are extensively used in a variety of sensor and actuator applications, where the coupling between mechanical and electrical fields are

of primary interest. They are also a promising set of materials for improved dynamic as well as non-volatile memory devices, where only the electrical properties are directly exploited. However, ferroelectrics are brittle, and their low fracture toughness (in the order of $1\,\mathrm{MPa\,m^{1/2}}$) makes them susceptible to cracking. In addition, ferroelectric materials exhibit electrical fatigue (loss of switchable polarization) under cyclic electrical loading and, due to the strong electro-mechanical coupling, sometimes mechanical fatigue as well. Conversely, the propagation of fatigue cracks hinders the performance of the devices and raises serious reliability concerns.

Ferroelectric fatigue is caused by a combination of electrical, mechanical and electrochemical processes, each of which has been claimed to be responsible for fatigue [1]. Several electrochemical mechanisms have been posited as the likely cause of polarization fatigue [2, e.g.], but no general consensus appears to have emerged as yet. Fatigue mechanisms variously include processes of distributed damage over the bulk (e. g., [3,4]) and processes of localized damage, including microcracks and ferroelectric-electrode interfaces (e.g., [5–7]). The proposed mechanisms include domain-wall pinning and inhibition of reversed domain nucleation [8,9,2]. The former mechanism is thought to play a dominant role in the bulk, whereas the latter mechanism is thought to operate primarily at or near electrode interfaces [10]. The relative roles of these and other mechanisms may depend on the frequency of the applied field [10]. At the atomic level, oxygen vacancies are likely to promote fatigue, e. g., by migrating under the action of the electric field to form extended defects that pin domain walls [11–13]. Purely mechanical mechanisms, such as microcracking, are also likely to play some role. Thus, fatigued ceramic specimens often contain scattered microcracks of size comparable to that of the grains [14,15]. Profuse microcrack clouds have been observed at the specimen edges and surrounding macroscopic cracks [16]. Macroscopic crack patterns are present in some fatigued ceramic specimens [17]. Severe cracking was also observed in barium titanate single crystals subjected to cyclic bipolar electric load [18]. Modelling work suggests that microcracking is indeed a cause of loss of polarization [6].

Experiments on crack propagation have been reported for samples loaded electrically, mechanically, or under combined loading, cyclic or static [19–22]. It is not uncommon for different experiments to lead to apparently contradictory conclusions [23], a testament to the complexity of the phenomenon of ferroelectric fatigue. On the other hand, a large body of experimental data concerns smooth samples, or samples without an initial pre-crack. In these experiments the main property of interest is the evolution of polarization, and often no special attention is given to the mechanical integrity of the sample. Epitaxially-grown thin films constitute a common configuration for tests involving smooth samples [24].

Despite these recent experimental and modelling advances, the precise nature

2

of the interactions between fracture, deformation and defect structures underlying ferroelectric fatigue is in need of further elucidation, and a physics-based multiscale model enabling the prediction of the fatigue life of ferroelectric devices is yet to emerge. Therefore, there remains a need for phenomenological and empirical models that can be experimentally validated and used in engineering design. In this vein, cohesive theories provide an effective means of modelling fatigue-crack nucleation and growth for arbitrary crack and specimen geometries and loading histories [25,26]. As noted by Nguyen *et al.* [25], the essential feature that a cohesive law must possess in order to model fatigue crack growth is *loading-unloading hysteresis*. By this simple but essential device, cohesive models of mechanical fatigue have been shown to account for deviations from Paris' law in metals such as are observed for short cracks and overloads [25]; and to predict fatigue-crack nucleation in smooth-surface metallic specimens [26]. The appealing feature of cohesive models of fatigue is that a single mechanistic, albeit empirical, model applies to nucleation and propagation, short and long cracks, and arbitrary loading histories.

Conventional cohesive models of fracture seek to describe the relation between cohesive tractions and opening displacements at the tip of a crack. Working by analogy, Gao *et al.* [27–29] have proposed the use of Dugdale-like models for the electric displacement in ferroelectric materials. In this paper, we further extend the concept of cohesive surface to ferroelectric materials by understanding it to be a surface of both *mechanical opening displacement and electric-potential discontinuity*. Correspondingly, we extend the concept of cohesive law to mean a general relation between the work-conjugate pairs: mechanical displacement and electric-potential discontinuity; and mechanical tractions and surface-charge density. Following Nguyen *et al.* [25], in order to model ferroelectric fatigue we endow the ferroelectric cohesive law with loading-unloading hysteresis. In order to simplify modelling, following [30] we make the additional assumption that the cohesive law derives from a potential that depends on a scalar effective electromechanical jump, which is a weighted norm of mechanical opening displacements and electric-potential jump.

Using a simple Smith-Ferrante monotonic envelope and an exponential-decay law of loading-unloading hysteresis we show that the model is able to qualitatively capture salient features of the experimental record including: the existence of a threshold nominal field for the onset of fatigue; the dependence of the threshold on the applied-field frequency; the dependence of fatigue life on the amplitude of the nominal field; and the dependence of the coercive field on the size of the component, or *size effect*.

2   Electromechanical cohesive laws

The essential structure of cohesive laws in ferroelectrics may be elucidated by recourse to a conventional Coleman-Noll argument (cf., [30] for an application to mechanical decohesion). In particular, the pairing between stress-like and deformation-like variables is determined by the internal-power identity or, equivalently, by the virtual-work identity. For a dielectric solid, this identity is [31–33]

$$\int_\Omega (\boldsymbol{\sigma} : \delta\boldsymbol{\epsilon} - \boldsymbol{D} \cdot \delta\boldsymbol{E})\, dV = \int_\Omega (\boldsymbol{b} \cdot \delta\boldsymbol{u} - \rho\, \delta\phi)\, dV + \int_{\partial\Omega} (\boldsymbol{t} \cdot \delta\boldsymbol{u} - \omega_{\mathrm{f}}\, \delta\phi)\, dS \ , \quad (1)$$

where Ω is the spatial domain occupied by the solid and $\partial\Omega$ is its boundary; $\boldsymbol{\sigma}$ is the stress;

$$\boldsymbol{\epsilon} = \frac{1}{2}(\nabla\boldsymbol{u} + \nabla\boldsymbol{u}^T) \qquad (2)$$

is the strain; $\boldsymbol{D}$ is the electric displacement;

$$\boldsymbol{E} = -\nabla\phi \qquad (3)$$

is the electric field; $\boldsymbol{b}$ is the body force; $\boldsymbol{u}$ is the displacement; ρ is the *free* charge density; ϕ is the electric potential; $\boldsymbol{t} = \boldsymbol{\sigma} \cdot \boldsymbol{n}$ is the surface traction; and $\omega_{\mathrm{f}} = -\boldsymbol{D} \cdot \boldsymbol{n}$ is the *free* surface charge per unit area. For a solid with a surface of discontinuity Γ, or cohesive surface, we have

$$
\begin{aligned}
\delta W_{\mathrm{ext}} &= \int_\Omega (\boldsymbol{b} \cdot \delta\boldsymbol{u} - \rho\delta\phi) dV + \int_{\partial\Omega} (\boldsymbol{t} \cdot \delta\boldsymbol{u} - \omega_{\mathrm{f}}\delta\phi) dS \\
&= \int_\Omega (\boldsymbol{b} \cdot \delta\boldsymbol{u} - \rho\delta\phi) dV + \int_{\partial\Omega} [(\boldsymbol{n} \cdot \boldsymbol{\sigma}) \cdot \delta\boldsymbol{u} + (\boldsymbol{n} \cdot \boldsymbol{D})\delta\phi] dS \\
&= \int_\Omega (\boldsymbol{b} \cdot \delta\boldsymbol{u} - \rho\delta\phi) dV + \int_{\Omega^\pm} [\nabla \cdot (\boldsymbol{\sigma} \cdot \delta\boldsymbol{u}) + \nabla \cdot (\boldsymbol{D}\delta\phi)] dV \\
&\quad + \int_\Gamma [(\boldsymbol{n} \cdot \boldsymbol{\sigma}) \cdot [\![\delta\boldsymbol{u}]\!] + (\boldsymbol{n} \cdot \boldsymbol{D})[\![\delta\phi]\!]] dS \ ,
\end{aligned}
$$

and consequently

$$\delta W_{\mathrm{int}} = \int_{\Omega^\pm} (\boldsymbol{\sigma} : \delta\boldsymbol{\varepsilon} - \boldsymbol{D} \cdot \delta\boldsymbol{E}) dV + \int_\Gamma [(\boldsymbol{n} \cdot \boldsymbol{\sigma}) \cdot \delta[\![\boldsymbol{u}]\!] + (\boldsymbol{n} \cdot \boldsymbol{D})\delta[\![\phi]\!]] dS \ . \quad (4)$$

For monotonic loading of the cohesive surface, these work-conjugacy relations naturally suggest a free energy per unit surface, or cohesive potential, of the

form $\Phi(\llbracket \boldsymbol{u} \rrbracket, \llbracket \phi \rrbracket, \boldsymbol{q})$ such that

$$\boldsymbol{t} = \frac{\partial \Phi}{\partial \llbracket \boldsymbol{u} \rrbracket} \ , \tag{5a}$$

$$-\omega_{\mathrm{f}} = \frac{\partial \Phi}{\partial \llbracket \phi \rrbracket} \ , \tag{5b}$$

where $\boldsymbol{q}$ is some suitable set of internal variables. A possible additional dependence of Φ on temperature is omitted for notational convenience. Thus, Φ depends both on the displacement and electric potential jumps across Γ and acts as a potential jointly for the mechanical tractions and the surface charge density.

It bears emphasis that the ferroelectric cohesive law (5a-5b) allows for an arbitrary coupling of the mechanical and electrical fields. It should also be carefully noted that the ferroelectric cohesive law describes the physics of *mechanical or electrical* decohesion and does not presume a particular form of the constitutive law governing the behavior in the bulk. In particular, it is possible to apply the ferroelectric cohesive law (5a-5b) in conjunction with Landau-Ginzburg-Devonshire models of domain switching (cf., e. g., [34]). The detailed boundary conditions on the crack faces are thought to greatly affect the fracture behavior of electrically driven crack growth [35]. For instance, partial discharge or charge separation effects have been suggested to play an important role in the vicinity of the crack tip [36]. The ferroelectric cohesive law (5a-5b) provides a useful framework for modelling those phenomena as well. Moreover, the ferroelectric cohesive law encodes the physics of decohesion, and thus can be tailored to represent any of the localized mechanisms of ferroelectric fatigue.

2.1 Ferroelectric fatigue cohesive law

As noted by Nguyen *et al.* [25], reversible cohesive laws do not predict crack advance under cyclic loading and, therefore, are insufficient for modelling fatigue. Instead, for a cohesive law to predict fatigue it must be irreversible and account for loading-unloading hysteresis. Loading-unloading irreversibility may be built into a cohesive law by means of the internal variable formalism (cf., e. g., [30]). The loading-unloading hysteresis model developed subsequently extends that of Nguyen *et al.* [25] to ferroelectric fatigue.

The modelling process is greatly simplified by the assumption that the cohesive potential Φ depends on the displacement and electric-potential jumps only through the effective electromechanical jump [37,30]

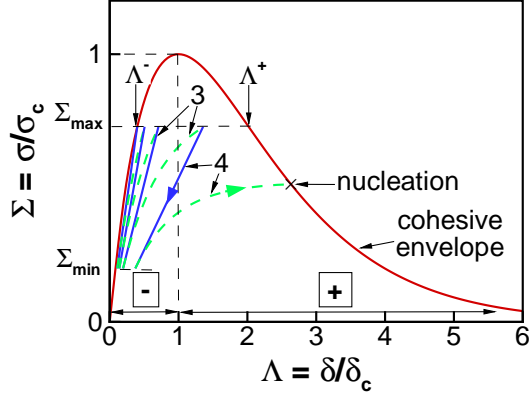$$\delta = \sqrt{{\delta_n}^2 + \beta^2 {\delta_s}^2 + \gamma^2 \psi^2} \ , \tag{6}$$

Fig. 1. Cyclic behavior predicted by the model and conventional definition of fatigue initiation.

i. e., by assuming

$$\Phi = \Phi(\delta, \boldsymbol{q}) \ , \tag{7}$$

where we write

$$\boldsymbol{\delta} = [\![\boldsymbol{u}]\!] \ , \tag{8a}$$
$$\delta_n = \boldsymbol{\delta} \cdot \boldsymbol{n} \ , \tag{8b}$$
$$\boldsymbol{\delta}_n = \delta_n \boldsymbol{n} \ , \tag{8c}$$
$$\delta_s = \sqrt{\boldsymbol{\delta}^2 - \delta_n{}^2} \ , \tag{8d}$$
$$\boldsymbol{\delta}_s = \boldsymbol{\delta} - \boldsymbol{\delta}_n = \delta_s \boldsymbol{s} \ , \tag{8e}$$
$$\psi = [\![\phi]\!], \tag{8f}$$

for the normal and tangential components of the opening displacement and the electric potential jump, respectively. The parameters β and γ assign different relative weights to normal and tangential opening displacements, thus differentiating between mode I and modes II and III of fracture; and to opening displacements and the electric potential jump, thus differentiating between mechanical and electrical fatigue.

An effective electromechanical flux may also be defined as

$$\sigma = \frac{\partial \Phi}{\partial \delta} \ . \tag{9}$$

Using the chain rule, (5a) and (5b) evaluate to

$$\boldsymbol{\tau} = \frac{\sigma}{\delta}[(1 - \beta^2)\delta_n \boldsymbol{n} + \beta^2 \boldsymbol{\delta}] = \frac{\sigma}{\delta}(\delta_n \boldsymbol{n} + \beta^2 \delta_s \boldsymbol{s}) = \tau_n \boldsymbol{n} + \tau_s \boldsymbol{s} \ , \tag{10a}$$
$$-\omega_{\mathrm{f}} = \frac{\sigma}{\delta}\gamma^2 \psi \ . \tag{10b}$$

We also note that

$$\sigma = \sqrt{\tau_n{}^2 + \tau_s{}^2/\beta^2 + \omega_{\mathrm{f}}{}^2/\gamma^2} \ . \tag{11}$$

6

Next we further specialize the preceding framework along the lines of the cohesive model of fatigue crack nucleation and growth proposed by Serebrinsky and Ortiz [26] and by Nguyen *et al.* [25]. The essential feature to include in the model is loading-unloading hysteresis. The specific scheme chosen to build hysteresis into the model is illustrated in Fig. 1. Monotonic loading is characterized by a cohesive law $\sigma(\delta)$, referred to as the monotonic envelope, which is characterized by the critical electromechanical flux σ_c and the critical electromechanical jump δ_c, and possibly an initial threshold σ_{th}. In contrast, cyclic loading is hysteretic and governed by the loading-unloading law:

$$\dot{\sigma} = \begin{cases} K_u \dot{\delta}, & \text{if } \dot{\delta} < 0 \\ K_l \dot{\delta}, & \text{if } \dot{\delta} > 0 \end{cases} , \tag{12}$$

where K_l and K_u are the loading and unloading incremental stiffnesses, respectively. Equivalently we may write

$$\dot{\sigma} = f_1(\dot{\delta}, K_l, K_u) \, \dot{\delta} , \tag{13}$$

with

$$f_1(\dot{\delta}, K_l, K_u) = \theta(\dot{\delta}) K_l + \theta(-\dot{\delta}) K_u , \tag{14}$$

where θ is the Heaviside step function. For definiteness, we assume unloading to take place towards the origin and K_u to be constant during unloading, Fig. 1. The value of K_u during an unloading event is determined by the values of σ and δ at the unloading point. Upon reloading, we additionally suppose that the reloading slope $K_l = d\sigma/d\delta$ decreases with increasing electromechanical jump as a result of interfacial degradation mechanisms occurring at the microscale. During unloading, a partial recovery of K_l is also allowed for. For definiteness we take

$$\dot{K}_l = \begin{cases} (K_l - K_u) \, \dot{\delta}/\delta_a, & \text{if } \dot{\delta} < 0 \\ -K_l \dot{\delta}/\delta_a, & \text{if } \dot{\delta} > 0 \end{cases} , \tag{15}$$

where δ_a is an intrinsic length of the material. Equivalently, we may write

$$\dot{K}_l = f_2(\dot{\delta}, K_l, K_u) \, \dot{\delta}/\delta_a , \tag{16}$$

with

$$f_2(\dot{\delta}, K_l, K_u) = -\theta(\dot{\delta}) K_l + \theta(-\dot{\delta})(K_l - K_u) . \tag{17}$$

Thus, $\boldsymbol{q} = (K_u, K_l)$ may be regarded as the internal variables of the model. An appealing feature of the model is the small number of parameters, namely: the constants defining the monotonic envelope, such as tensile strength and toughness; the coupling constants β and γ; and the intrinsic length δ_a.

The cyclic behavior predicted by the model just outlined is shown schematically in Fig. 1 for cycling between constant maximum and minimum effective

electromechanical fluxes. Thus, for monotonic loading the cohesive surface follows the monotonic envelope. Upon cyclic loading, the cohesive stiffness of the surface degrades steadily and, after a certain number of cycles, the $\big(\sigma(t), \delta(t)\big)$ curve meets the monotonic envelope. *We identify this event with the end of the fatigue life of the material.* Indeed, once the curve $\big(\sigma(t), \delta(t)\big)$ meets the monotonic envelope, the material can no longer sustain a loading cycle of the same amplitude and, consequently, fails catastrophically under load control.

2.2 Bulk behavior

A closed set of governing equations may be obtained by appending a suitable bulk energy density to the cohesive model just described and considering the corresponding gradient flow. Following Zhang and Bhattacharya [38], we assume a bulk energy density of the form

$$W(\boldsymbol{P}, \boldsymbol{\epsilon}) = W_1(\boldsymbol{P}) + W_2(\boldsymbol{\epsilon}) + W_3(\boldsymbol{P}, \boldsymbol{\epsilon}) \ , \tag{18}$$

where the polarization energy density $W_1(\boldsymbol{P})$ is polynomial of degree eight in the polarization $\boldsymbol{P}$, with multiple wells corresponding to the different variants of the material, and

$$W_2(\boldsymbol{\epsilon}) = \tfrac{1}{2}\boldsymbol{\epsilon} : \boldsymbol{C} : \boldsymbol{\epsilon} \ , \tag{19a}$$

$$W_3(\boldsymbol{P}, \boldsymbol{\epsilon}) = -\tfrac{1}{2}\boldsymbol{\epsilon} : (\boldsymbol{P} \cdot \boldsymbol{B} \cdot \boldsymbol{P}) \ , \tag{19b}$$

are the strain and mixed energy densities, respectively. Following Shu and Bhattacharya [34], we additionally assume the total energy of the body to be of the form

$$E[\boldsymbol{P}, \boldsymbol{u}, \phi] = \int_\Omega \left(W(\boldsymbol{P}, \boldsymbol{\epsilon}) + \frac{\epsilon_0}{2}|\nabla\phi|^2 \right) d\Omega \ , \tag{20}$$

where W is the bulk energy density and $\epsilon_0 = 8.854 \times 10^{-12}\,\mathrm{F/m}$ is the permeability of vacuum and the energy of domain walls is neglected for simplicity. A gradient flow of this energy results in the time-dependent Ginzburg-Landau equations

$$\mu\,\dot{\boldsymbol{P}} = -\frac{\partial W}{\partial \boldsymbol{P}}(\boldsymbol{P}, \boldsymbol{\epsilon}) + \boldsymbol{E} \ , \tag{21}$$

$$\nabla \cdot (\boldsymbol{P} + \epsilon_0 \boldsymbol{E}) = 0 \ , \tag{22}$$

$$\nabla \cdot \frac{\partial W}{\partial \boldsymbol{\epsilon}}(\boldsymbol{P}, \boldsymbol{\epsilon}) = \boldsymbol{0} \ , \tag{23}$$

where $1/\mu$ is the mobility. In these equations we recognize an equation of evolution for the polarization $\boldsymbol{P}$, Gauss' law, and the equation of mechanical

equilibrium, respectively. At equilibrium $\dot{\boldsymbol{P}} = 0$ and Eq. (21) reduces to

$$-\frac{\partial W}{\partial \boldsymbol{P}}(\boldsymbol{P}, \boldsymbol{\epsilon}) + \boldsymbol{E} = 0 \ , \tag{24}$$

which is also obtained in the formal limit of $\mu \to 0$. Eqs. (21), (22) and (23), in conjunction with (3) and (2), define a closed initial-boundary-value problem for the polarization $\boldsymbol{P}$, the electrostatic potential ϕ and the mechanical displacement $\boldsymbol{u}$.

3 Experimental validation

In order to make contact with experiment and assess the validity of the model we consider a simple test configuration consisting of an infinite slab of thickness u acted upon by an oscillatory voltage differential $\Delta\phi_T$ across the slab and otherwise stress free. The mid plane of the slab is a weak interface governed by the cohesive model proposed in § 2. In order to simplify the analysis, we assume all fields to be uniform outside the cohesive interface. This assumption has the effect of reducing the initial-boundary-value problem (21), (22) and (23) to a simple set of ordinary differential equations in time. Taking the cohesive plane to coincide with the (x_1, x_2)-coordinate plane and assuming uniaxial strain conditions, $\epsilon_{11} = \epsilon_{22} = \epsilon_{12} = \epsilon_{13} = \epsilon_{23} = 0$, the various bulk energy densities reduce to

$$W_1(P_3) = \frac{a_1}{2}P_3^2 + \frac{a_2}{4}P_3^4 + \frac{a_3}{6}P_3^6 \ , \tag{25a}$$

$$W_2(\epsilon_{33}) = \frac{c_1}{2}\epsilon_{33}^2 \ , \tag{25b}$$

$$W_3(P_3, \epsilon_{33}) = -\frac{b_1}{2}\epsilon_{33}P_3^2 \ , \tag{25c}$$

where a_1, a_2, a_3, c_1 and b_1 are empirical constants. The transverse stress follows from these expressions as

$$\sigma_{33} = c_1\epsilon_{33} - \frac{b_1}{2}P_3^2 \ . \tag{26}$$

The stress-free condition $\sigma_{33} = 0$ then gives the transverse strain as

$$\epsilon_{33} = \frac{b_1}{2c_1}P_3^2 \ . \tag{27}$$

Using this identity, (21) reduces to

$$\mu\dot{P}_3 + a_1 P_3 + \left(a_2 - \frac{b_1^2}{2c_1}\right)P_3^3 + a_3 P_3^5 = E_3 \ . \tag{28}$$
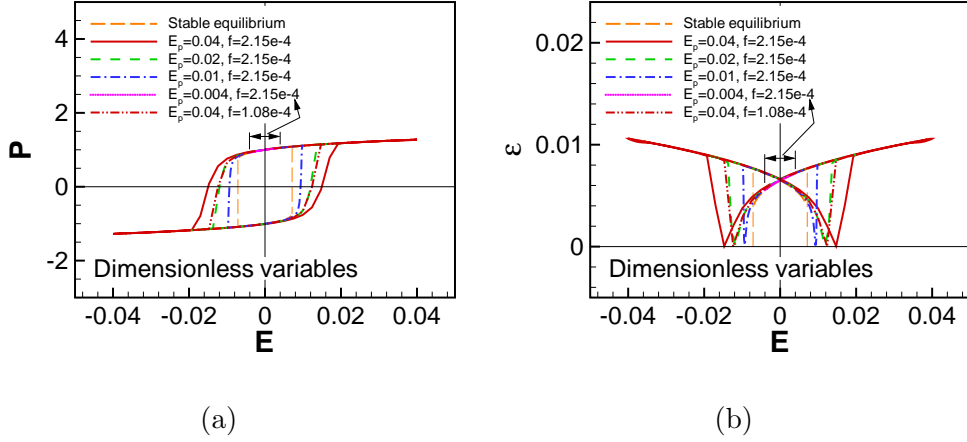
Fig. 2. Bulk response for different field amplitudes and frequencies. a) $P - E$ hysteresis loops. b) $\epsilon - E$ butterfly loops.

From Eq. (22) and the boundary conditions, at the cohesive interface we additionally have

$$-\omega_{\mathrm{f}} = P_3 + \epsilon_0 E_3 \ , \tag{29a}$$

$$\psi = E_3\, u + \Delta\phi_T \ . \tag{29b}$$

Finally, the coupled electromechanical cohesive law specializes to

$$\dot{\sigma} = f_1(\dot{\delta}, K_1, \sigma/\delta)\, \dot{\delta} \ , \tag{30a}$$

$$\dot{K}_1 = f_2(\dot{\delta}, K_1, \sigma/\delta)\, \dot{\delta} \ , \tag{30b}$$

$$\gamma^2 \left(\frac{P_3 u - \epsilon_0 \Delta\phi_T}{\sigma u \gamma^2 - \epsilon_0 \delta} \right)^2 = 1 \ , \tag{30c}$$

where

$$\delta = \gamma|\psi| \ , \tag{31a}$$

$$\sigma = \frac{1}{\gamma}|\omega| \ . \tag{31b}$$

In calculations we enforce the constraint (30c) in differential form and solve the resulting system of ordinary differential equations in time by means of a fourth-order Runge Kutta algorithm. In implementing this algorithm, care must be exercised in order to resolve ambiguities in the selection of branches and the handling of singularities in the response functions as δ tends to zero. In the sequel, $P = P_3$ and similarly for other vector quantities, and $\epsilon = \epsilon_{33}$.

For sufficiently high applied field, the calculated response exhibits characteristic hysteresis loops in a $P - E$ plot, and butterfly loops in a $\epsilon - E$ plot. These loops are shown in Fig. 2 for several values of the peak electric field E_{p} and

10

a_1	a_2	a_3	b_1	c_1	ϵ_0	γ	μ
-0.007	-0.009	0.0261	1.4282	185	0.131	800	1

Table 1
Values of the model parameters.

the applied field frequency f. Several aspects of the bulk response are noteworthy. Thus, below a minimum value of E_p no switching occurs, and the sign of the polarization remains constant in time. The rate-dependency introduced by the time-dependent Ginzburg-Landau equation is evident in Fig. 2. In the limit of $\mu = 0$ or, equivalently, of a small frequency of the applied field, this rate dependency is removed and an equilibrium loop is obtained. For nonzero μ the bulk response depends on the applied-field frequency.

The predictions of the model in the example just described can now be compared with experimental data by way of validation. In order to facilitate comparisons for different materials we introduce the following normalization constants for the variables: polarization, P_{ref}; stress, elastic constants, c_{ref}; permittivity, $\epsilon_{0ref} = P_{ref}^2/c_{ref}$; electric field, $E_{ref} = P_{ref}/\epsilon_{0ref}$; thickness, displacements, $L_{ref} = \delta_a$; potential, $\phi_{ref} = E_{ref}L_{ref}$; time $t_{ref} = \mu P_{ref}^2/c_{ref}$; energy density coefficients, $b_{ref} = a_{1ref} = c_{ref}/P_{ref}$, $a_{2ref} = a_{1ref}/P_{ref}^2$, $a_{3ref} = a_{1ref}/P_{ref}^4$; coefficient $\gamma_{ref} = P_{ref}/c_{ref}$; cohesive stiffness $K_{ref} = c_{ref}/L_{ref}$. Dimensionless variables are used in the calculations, and the parameters and material constants are summarized in Table 3. We have selected material constants for the bulk model readily available from the literature [38], which correspond to BaTiO$_3$. The initial conditions are $P_{30} = 1$, $K_{10} = 2311$, and δ_0 and σ_0 are chosen to give a ratio $K_{10}/K_{u0} = 0.99$.

Typical experimental data are given in the form

$$P_x = P_x(E_p^*, N, u) , \tag{32}$$

where $E_p^* = -\Delta\phi_p/u$ is the peak *nominal* electric field, which should be carefully differentiated from the peak *actual* field E_p in the material, N is the cycle number, and P_x is a measure of the polarization state of the material, typically the remanent polarization P_r but also sometimes P_{sw}, the switching polarization. From these data, a relation $E_f^*(N, u)$, or the inverse relation $N_f(E_p^*, u)$, can be derived by solving the equation

$$\frac{P_x(E_p^*, N, u)}{P_x(E_p^*, 1, u)} = 1 - C, \tag{33}$$

where C is the loss of polarization due to fatigue. We shall take these fatigue maps as the basis for the validation of the model.

As expected, the predicted fatigue behavior depends critically on whether switching occurs. In the presence of switching, the interface degrades upon
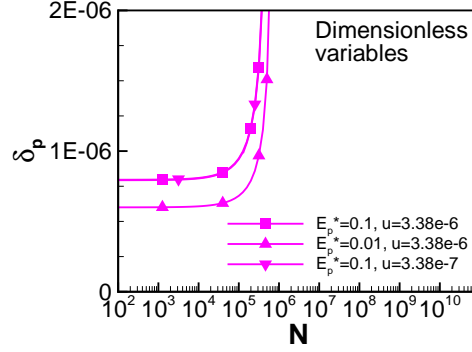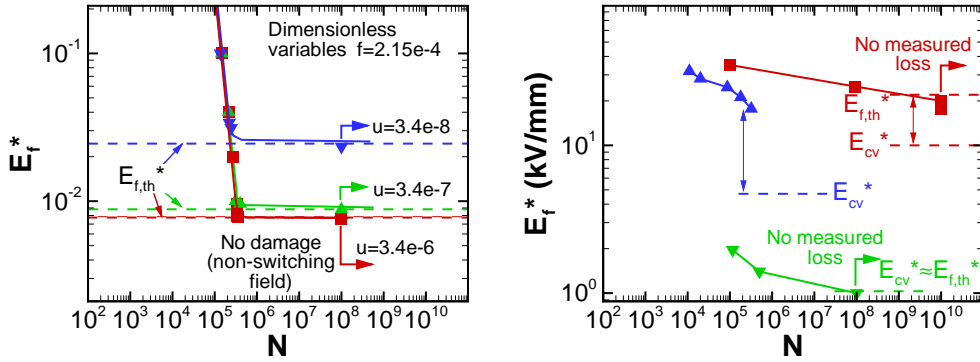
Fig. 3. Evolution with number of cycles of the peak effective opening displacement δ_{p}.
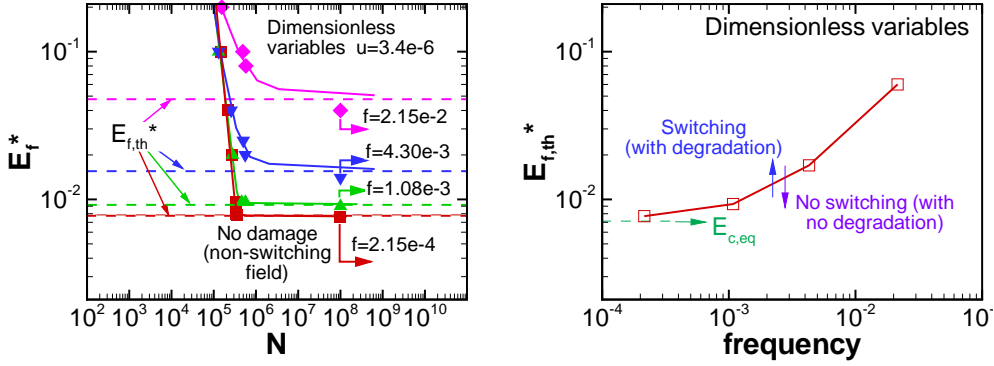

(a) Calculated. In all cases, $E^*_{\mathrm{f,th}} = E^*_{\mathrm{cv}}$.

(b) Experimental (all in PZT), loss=10%. ■: Grossmann *et al.* [39], ▼: Nuffer *et al.* [1], ▲: Mihara *et al.* [40]. In all cases, $E^*_{\mathrm{f,th}} \geq E^*_{\mathrm{cv}}$.

Fig. 4. Fatigue life as a function of nominal field and thickness.

cycling and the peak value of δ increases monotonically with the number of cycles, Fig. 3. The increase in δ is initially slow and accelerates markedly in the last stages of the fatigue life of the material. The rate of damage accumulation increases with the amplitude of the nominal field. Correspondingly, as the interface degrades the switching capability and the actuation strain are impaired.

The calculated fatigue map, for small frequencies for which rate-dependency is negligible, is shown in Fig. 4(a). It is immediately apparent from this map that for each thickness u there is a threshold amplitude $E^*_{\mathrm{f,th}}$ below which fatigue does not occur. Specifically, fatigue occurs if the nominal field E^*_{p} is sufficiently strong to cause switching, and fatigue does not occur otherwise. Thus, the fatigue threshold $E^*_{\mathrm{f,th}}$ coincides with the nominal coercive field E^*_{cv} for the virgin material. For nominal fields above the fatigue threshold $E^*_{\mathrm{f,th}}$,

12

(a) Fatigue life as a function of applied field frequency.

(b) Effect of frequency on nominal threshold field.

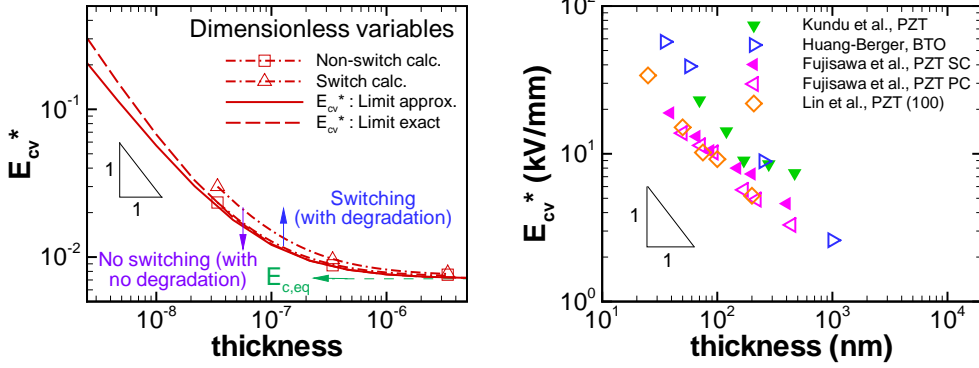Fig. 5. Effect of applied field frequency on fatigue properties.

the model predicts the fatigue life N_f to shorten with increasing nominal field amplitude E_p^*. This dependency is well approximated by the power law

$$N_f = A E_p^{*n} \, , \tag{34}$$

with exponent $-n \approx 2.8$.

For bulk-like samples and high frequencies, the fatigue life has a steeper dependency on the applied field, as shown in Fig. 5(a). It is readily verified that the transition from non-switching to switching bulk behavior, as the applied field increases, appears smoother as the field frequency increases, thus leading to the calculated fatigue behavior. In addition, $E_{f,th}^*$ can be greatly in excess of E_{cv}^*, as Fig. 5(b) shows. It also indicates that the low frequency limit is attained for the lowest frequency used.

Corresponding experimental data for smooth tetragonal PZT samples [39,1,40] are shown in Fig. 4(b) for purposes of comparison. Evidently, the predicted existence of a fatigue threshold and the reduction in fatigue life with nominal field amplitude are consistent with the data. The nominal fatigue threshold $E_{f,th}^*$ is indeed observed to be greater than or equal to the nominal coercive field E_{cv}^*, as obtained from the respective hysteresis loops. Besides these experiments where no microcracking was observed or analyzed, the relation between switching and fatigue has also been established on indented and precracked samples by the experiments of Zhu *et al.* [22]. Thus, switching appears as a necessary (though not sufficient) condition for electrical fatigue, regardless of the fatigue mechanism operating. It should be noted that there are other methods, alternative to electric fatigue, to suppress polarization (e. g., [41]). The experimental data shown in Fig. 4(b) is also suggestive of power-law behavior (see Eq. (34)) with exponents in the range $-n \approx 0.16 - 0.24$. The difference with the predicted value is due to the choice bulk behavior, which has no

(a) Calculated. Determined from Fig. 4(a): △: lowest values of E_p^* with switching behavior, □: highest values of E_p^* with non-switching behavior. Determined from models with $K_l = K_u = \text{const.}$: $-$: approximate model, $--$: exact model.

(b) Experimental. ◀, ◁: Fujisawa *et al.* [43], ▼: Kundu and Lee [44], ▷: Huang and Berger [45], ◇: Lin *et al.* [46].

Fig. 6. Nominal electric field required for switching.

dependence of the actual coercive field on actual field amplitude for $E_p > E_c$, and not to the cohesive model. The dependence of the fatigue threshold on the applied field frequency, with high frequencies delaying the onset of fatigue, was established by Grossmann *et al.* [39].

It is worth mentioning that some alternatives were developed to suppress polarization fatigue, including using conducting oxide electrodes [42]. Such devices can be modelled by an interface with a large value of δ_a, which would lead to a minor fatigue effect. In the limit of $\delta_a \to \infty$, fatigue would be completely absent.

In order to exhibit the size effect predicted by the model, Fig. 6(a) plots specimen thickness against the minimum value of E_p^* for which switching occurs, and the maximum value of E_p^* for which switching does not occur. Insight into this dependence may be derived by analyzing the equilibrium case of $\dot{P} = 0$ in Eq. (21). In this case, the governing equations reduce to

$$E = a_1 P + \left(a_2 - \frac{b_1^2}{2c_1} \right) P^3 + a_3 P^5 \ , \tag{35a}$$

$$P = E(K_u \gamma^2 u - \epsilon_0) + K_u \gamma^2 \Delta \phi_T \ . \tag{35b}$$

For a virgin material, i. e., a material with high K_u, it is readily shown that the nominal coercive field E_{cv}^* required for switching is of the form

$$E_{cv}^*(u) = \Delta \phi_c(u)/u \sim E_{ceq} + (P_{ceq} + \epsilon_0 E_{ceq})/(K_u \gamma^2 u) \ . \tag{36}$$

14

where $E_{\text{ceq}} = 0.007129$. This relation is plotted in Fig. 6(a) along with the exact calculated values of $E_{\text{cv}}^*(u)$ from Eqs. (35). It is noteworthy that E_{cv}^* decreases monotonically with size u to a limiting value E_{ceq} characteristic of large components. Conversely, E_{cv}^* increases as u^{-1} for a small component thickness. This prediction of the model is born out by the experimental data, Fig. 6(b), which is consistent with the $E_{\text{cv}}^* \sim u^{-1}$ scaling behavior. By contrast, the size effect above the nominal fatigue threshold $E_{\text{f,th}}^*$ is negligible, Fig. 4(a). This lack of sensitivity to the component size is also visible in the evolution of δ_{p}, Fig. 3. Thus, the main effect of component size is on the ability of the material to switch and, by extension, on the nominal fatigue threshold $E_{\text{f,th}}^*$. It should be noted that alternative explanations for the size effect have been proposed, including **depolarization fields [47,48],** epitaxial stress effects [49,45] and variants of a conductive layer next to the ferroelectric-electrode interface [50,51].

4   Summary and concluding remarks

We have presented a model of electro-mechanical ferroelectric fatigue based on the postulate of a ferroelectric cohesive law that: couples mechanical displacement and electric-potential discontinuity to mechanical tractions and surface-charge density; and exhibits a monotonic envelope and loading-unloading hysteresis. In conjunction with a constitutive model accounting for domain switching, the electro-mechanical cohesive fatigue law is able to induce ferroelectric fatigue by the following mechanism: as degradation proceeds, the surface of electromechanical discontinuity absorbs an increasingly large amount of the displacement and/or electric potential difference, thereby unloading the bulk and hindering switching. We identify the end of the fatigue life with the time at which the material loses its ability to sustain loading/applied field cycles of a certain constant amplitude. We have compared selected predictions of the model with experimental data for a simple test configuration consisting of an infinite slab acted upon by an oscillatory voltage differential across the slab and otherwise stress free. The model captures salient features of the experimental record including: the existence of a threshold nominal field for the onset of fatigue; the dependence of the threshold on the applied-field frequency; the dependence of fatigue life on the amplitude of the nominal field; and the dependence of the coercive field, and thus of the fatigue threshold, on the size of the component, or *size effect*. Our results seem to indicate that planar-like regions affected by cycling may lead to the observed fatigue in tetragonal PZT.

The ability of the model to predict the observed size effect stems directly from the fact that cohesive laws introduce a *characteristic or intrinsic material length scale*. Hence, in the present model the size effect is a material property and a direct consequence of material behavior. This is in contrast to other

explanations of the size effect found in the literature (e. g., [50,51,49]), where the length scale is often structural.

In closing, we emphasize that the primary focus of this study has been to investigate qualitative trends and no systematic attempt has been made to optimize fit to the experimental data. It is conceivable that good quantitative agreement with the data could be obtained by some extensions and careful calibration of the model, including full finite element calculations; the use of more accurate bulk constitutive relations; and a systematic identification of aspects of the cohesive law such as the precise shape of the monotonic envelope and of the loading-unloading law.

Acknowledgments

References

[1] J. Nuffer, D. C. Lupascu, J. Rödel, Damage evolution in ferroelectric PZT induced by bipolar electric cycling, Acta Mater. 48 (2000) 3783–3794.

[2] A. K. Tagantsev, I. Stolichnov, E. L. Colla, N. Setter, Polarization fatigue in ferroelectric films: Basic experimental findings, phenomenological scenarios, and microscopic features, J. Appl. Phys. 90 (3) (2001) 1387–1402.

[3] U. Robels, G. Arlt, Domain wall clamping in ferroelectrics by orientation of defects, J. Appl. Phys. 73 (7) (1993) 3454–3460.

[4] W. L. Warren, D. Dimos, B. A. Tuttle, R. D. Nasby, G. E. Pike, Electronic domain pinning in $Pb(Zr,Ti)O_3$ thin films and its role in fatigue, Appl. Phys. Lett. 65 (8) (1994) 1018–1020.

[5] J. F. Scott, C. A. Araujo, B. M. Melnick, L. D. Mcmillan, R. Zuleeg, Quantitative measurement of space-charge effects in lead zirconate-titanate memories, J. Appl. Phys. 70 (1) (1991) 382–388.

[6] S. J. Kim, Q. Jiang, Microcracking and electric fatigue of polycrystalline ferroelectric ceramics, Smart Mat. Struct. 5 (3) (1996) 321–326.

[7] I. Stolichnov, A. Tagantsev, N. Setter, J. S. Cross, M. Tsukada, Top-interface-controlled switching and fatigue endurance of $(Pb,La)(Zr,Ti)O_3$ ferroelectric capacitors, Appl. Phys. Lett. 74 (23) (1999) 3552–3554.

[8] W. L. Warren, D. Dimos, R. M. Waser, Degradation mechanisms in ferroelectric and high-permittivity perovskites, MRS Bull. 21 (7) (1996) 40–45.

[9] D. Damjanovic, Ferroelectric, dielectric and piezoelectric properties of ferroelectric thin films and ceramics, Rep. Prog. Phys. 61 (9) (1998) 1267–1324.

[10] E. L. Colla, D. V. Taylor, A. K. Tagantsev, N. Setter, Discrimination between bulk and interface scenarios for the suppression of the switchable polarization (fatigue) in $Pb(Zr,Ti)O_3$ thin films capacitors with Pt electrodes, Appl. Phys. Lett. 72 (19) (1998) 2478–2480.

[11] M. Dawber, J. F. Scott, A model for fatigue in ferroelectric perovskite thin films, Appl. Phys. Lett. 76 (8) (2000) 1060–1062.

[12] M. Dawber, J. F. Scott, Addendum: "A model for fatigue in ferroelectric perovskite thin films" [Appl. Phys. Lett. 76, 1060 (2000), Appl. Phys. Lett. 76 (24) (2000) 3655–3655.

[13] Y. Xiao, The influence of oxygen vacancies on domain patterns in ferroelectric perovskites, Ph.D. thesis, California Institute of Technology (September 2004).

[14] Q. Y. Jiang, L. E. Cross, Effects of porosity on electric fatigue behavior in PLZT and PZT ferroelectric ceramics, J. Mater. Sci. 28 (16) (1993) 4536–4543.

[15] Q. Y. Jiang, W. W. Cao, L. E. Cross, Electric fatigue in lead zirconate titanate ceramics, J. Amer. Ceram. Soc. 77 (1) (1994) 211–215.

[16] J. Nuffer, D. C. Lupascu, J. Rodel, Microcrack clouds in fatigued electrostrictive 9.5/65/35 PLZT, J. European Ceram. Soc. 21 (10-11) (2001) 1421–1423.

[17] J. Nuffer, D. C. Lupascu, A. Glazounov, H. Kleebe, J. Rödel, Microstructural modifications of ferroelectric lead zirconate titanate ceramics due to bipolar electric fatigue, J. European Ceram. Soc. 22 (13) (2002) 2133–2142.

[18] E. Burcsu, Investigation of large strain actuation in barium titanate, Ph.D. thesis, California Institute of Technology (May 2001).

[19] H. C. Cao, A. G. Evans, Electric-field-induced fatigue crack growth in piezoelectrics, J. Amer. Ceram. Soc. 77 (7) (1994) 1783–1786.

[20] C. S. Lynch, L. Chen, Z. Suo, R. M. McMeeking, W. Yang, Crack growth in ferroelectric ceramics driven by cyclic polarization switching, Journal of Intelligent Material Systems and Structures 6 (2) (1995) 191–198.

[21] C. S. Lynch, W. Yang, L. Collier, Z. Suo, R. M. McMeeking, Electric field induced cracking in ferroelectric ceramics, Ferroel. 166 (1995) 11–30.

[22] T. Zhu, F. Fang, W. Yang, Fatigue crack growth in ferroelectric ceramics below the coercive field, J. Mater. Sci. Lett. 18 (1999) 1025–1027.

[23] D. Fang, K. S. Ai, J. Liu, Electromechanical deformation and fracture of piezoelectric/ferroelectric materials, Acta Mech. Sin. 17 (2001) 193–213.

[24] T. M. Shaw, S. Trolier-McKinstry, P. C. McIntyre, The properties of ferroelectric films at small dimensions, Ann. Rev. Mat. Sci. 30 (2000) 263–298.

[25] O. Nguyen, E. A. Repetto, M. Ortiz, R. Radovitzky, A cohesive model of fatigue crack growth, Int. J. Fract. 110 (4) (2001) 351–369.

[26] S. Serebrinsky, M. Ortiz, A hysteretic cohesive-law model of fatigue-crack nucleation, Scripta Mater., in press (2005).

[27] H. J. Gao, T. Y. Zhang, P. Tong, Local and global energy release rates for an electrically yielded crack in a piezoelectric ceramic, J. Mech. Phys. Sol. 45 (4) (1997) 491–510.

[28] C. C. Fulton, H. Gao, Microstructural modeling of ferroelectric fracture, Acta Mater. 49 (11) (2001) 2039–2054.

[29] C. C. Fulton, H. J. Gao, Effect of local polarization switching on piezoelectric fracture, J. Mech. Phys. Sol. 49 (4) (2001) 927–952.

[30] M. Ortiz, A. Pandolfi, Finite deformation irreversible cohesive elements for three-dimensional crack-propagation analysis, Int. J. Numer. Meth. Eng. 44 (9) (1999) 1267–1282.

[31] Z. Suo, C.-M. Kuo, D. M. Barnett, J. R. Willis, Fracture mechanics for piezoelectric ceramics, J. Mech. Phys. Sol. 40 (4) (1992) 739–765.

[32] C. M. Landis, A new finite-element formulation for electromechanical boundary value problems, Int. J. Numer. Meth. Eng. 55 (5) (2002) 613–628.

[33] Z. Suo, X. Gong, Reliability of ceramic multilayer actuators: a nonlinear finite element simulation, J. Mech. Phys. Sol. 44 (1996) 751–769.

[34] Y. C. Shu, K. Bhattacharya, Domain patterns and macroscopic behaviour of ferroelectric materials, Phil. Mag. B 81 (12) (2001) 2021–2054.

[35] S. Li, On saturation-strip model of a permeable crack in a piezoelectric ceramic, Acta Mech. 165 (1-2) (2003) 47–71.

[36] R. M. McMeeking, Towards a fracture mechanics for brittle piezoelectric and dielectric materials, Int. J. Fract. 108 (1) (2001) 25–41.

[37] G. T. Camacho, M. Ortiz, Computational modelling of impact damage in brittle materials, Int. J. Sol. Struct. 33 (20-22) (1996) 2899–2938.

[38] W. Zhang, K. Bhattacharya, A computational model of ferroelectric domains. Part I: model formulation and domain switching, Acta Mater. 53 (1) (2005) 185–198.

[39] M. Grossmann, D. Bolten, O. Lohse, U. Boettger, R. Waser, S. Tiedke, Correlation between switching and fatigue in $PbZr_{0.3}Ti_{0.7}O_3$ thin films, Appl. Phys. Lett. 77 (12) (2000) 1894–1896.

[40] T. Mihara, H. Watanabe, C. A. P. De Araujo, Polarization fatigue characteristics of sol-gel ferroelectric $Pb(Zr_{0.4}Ti_{0.6})O_3$ thin-film capacitors, Jap. J. Appl. Phys., Part 1 – Regular Papers, Short Notes Rev. Papers 33 (7A) (1994) 3996–4002.

[41] W. L. Warren, D. Dimos, B. A. Tuttle, G. E. Pike, R. W. Schwartz, P. J. Clews, D. C. Mcintyre, Polarization suppression in $Pb(Zr,Ti)O_3$ thin-films, J. Appl. Phys. 77 (12) (1995) 6695–6702.

[42] J. J. Lee, C. L. Thio, S. B. Desu, Electrode contacts on ferroelectric $Pb(Zr_xTi_{1-x})O_3$ and $SrBi_2Ta_2O_9$ thin films and their influence on fatigue properties, J. Appl. Phys. 78 (8) (1995) 5073–5078.

[43] H. Fujisawa, S. Nakashima, K. Kaibara, M. Shimizu, H. Niu, Size effects of epitaxial and polycrystalline $Pb(Zr,Ti)O_3$ thin films grown by metalorganic chemical vapor deposition, Jap. J. Appl. Phys., Part 1 – Regular Papers, Short Notes Rev. Papers 38 (9B) (1999) 5392–5396.

[44] T. K. Kundu, J. Y.-M. Lee, Thickness dependence of the time dependent dielectric breakdown characteristics of $Pb(Zr,Ti)O_3$ thin film capacitors for memory device applications, Jap. J. Appl. Phys., Part 1 – Regular Papers, Short Notes Rev. Papers 39 (6A) (2000) 3488–3491.

[45] G. F. Huang, S. Berger, Combined effect of thickness and stress on ferroelectric behavior of thin $BaTiO_3$ films, J. Appl. Phys. 93 (5) (2003) 2855–2860.

[46] C. H. Lin, P. A. Friddle, C. H. Ma, A. Daga, H. D. Chen, Effects of thickness on the electrical properties of metalorganic chemical vapor deposited $Pb(Zr,Ti)O_3$ (25-100 nm) thin films on $LaNiO_3$ buffered Si, J. Appl. Phys. 90 (3) (2001) 1509–1515.

[47] P. Wurfel, I. P. Batra, Depolarization-field-induced instability in thin ferroelectric films – Experiment and theory, Phys. Rev. B 8 (11) (1973) 5126–5133.

[48] R. R. Mehta, B. D. Silverman, J. T. Jacobs, Depolarization fields in thin ferroelectric films, J. Appl. Phys. 44 (8) (1973) 3379–3385.

[49] N. A. Pertsev, J. Rodríguez Contreras, V. G. Kukhar, B. Hermanns, H. Kohlstedt, R. Waser, Coercive field of ultrathin $PbZr_{0.52}Ti_{0.48}O_3$ epitaxial films, Appl. Phys. Lett. 83 (16) (2003) 3356–3358.

[50] J. F. M. Cillessen, M. W. J. Prins, R. M. Wolf, Thickness dependence of the switching voltage in all-oxide ferroelectric thin-film capacitors prepared by pulsed laser deposition, J. Appl. Phys. 81 (6) (1997) 2777–2783.

[51] A. K. Tagantsev, I. A. Stolichnov, Injection-controlled size effect on switching of ferroelectric thin films, Appl. Phys. Lett. 74 (9) (1999) 1326–1328.